AGU PUBLICATIONS

Geophysical Research Letters

RESEARCH LETTER
10.1002/2015GL064992

Key Points:
- Propagation modeling improves significantly using ensembles of realistically perturbed analyses
- Small-scale fluctuations are not always necessary to improve infrasound propagation modeling
- Uncertainties in wind dominate the variation of the effective sound speed

Supporting Information:
- Supporting Information S1
- Figures S5

Correspondence to:
P. S. M. Smets,
p.s.m.smets@tudelft.nl

Citation:
Smets, P. S. M., L. G. Evers, S. P. Näsholm, and S. J. Gibbons (2015), Probabilistic infrasound propagation using realistic atmospheric perturbations, *Geophys. Res. Lett.*, *42*, 6510–6517, doi:10.1002/2015GL064992.

Received 30 JUN 2015
Accepted 16 JUL 2015
Accepted article online 20 JUL 2015
Published online 6 AUG 2015

Probabilistic infrasound propagation using realistic atmospheric perturbations

P. S. M. Smets[1,2], L. G. Evers[1,2], S. P. Näsholm[3], and S. J. Gibbons[3]

[1]Department of Geoscience and Engineering, Faculty of Civil Engineering and Geosciences, Delft University of Technology, Delft, Netherlands, [2]Department Seismology and Acoustics, Royal Netherlands Meteorological Institute (KNMI), De Bilt, Netherlands, [3]NORSAR, Kjeller, Norway

Abstract This study demonstrates probabilistic infrasound propagation modeling using realistic perturbations. The ensembles of perturbed analyses, provided by the European Centre for Medium-Range Weather Forecasts (ECMWF), include error variances of both model and assimilated observations. Ensemble spread profiles indicate a yearly mean effective sound speed variation of up to 8 ms^{-1} in the stratosphere, exceeding occasionally 25 ms^{-1} for a single ensemble set. It is shown that errors in point estimates of effective sound speed are dominated by variations in wind strength and direction. One year of large mining explosions in the Aitik mine, northern Sweden, observed at infrasound array IS37 in northern Norway are simulated using 3-D ray tracing. Probabilistic propagation modeling using the ensembles demonstrates that small-scale fluctuations are not always necessary to improve the match between predictions and observations.

1. Introduction

The state of the atmosphere is of utmost importance for infrasound propagation. In infrasound propagation modeling, still, the true state of the atmosphere is usually represented by the analysis. The analysis is the best deterministic estimate of the atmosphere using a data assimilation system consisting of a general circulation model (GCM).

General circulation models (GCMs) are advanced numerical models describing the physical state of the atmosphere and/or ocean, simulating the response of the global climate system. GCMs are smooth, designed to suppress unbalanced motion associated with, e.g., internal gravity waves, to allow longer time steps [*Shutts and Vosper*, 2011]. In general, GCMs have to deal with two disadvantages: parameterisation and feedback mechanisms of different processes [*Houghton et al.*, 1997; *Randall et al.*, 2007]. GCMs are limited in resolution relative to the scale for most impact assessments, e.g., clouds or gravity waves. Therefore, the effects of smaller length scale processes must be averaged over larger regions. This is referred to as parameterisation. Feedback mechanisms become an issue at the boundary of the model, where signals will be damped to avoid unwanted reflections. This results in a less physical representation but enhancement in model stability. Consequentially, GCM limitations influence the simulation of infrasound propagation, resulting in the lack of simulated arrivals due to fine-scale structure in wind and temperature [*Chunchuzov et al.*, 2005; *Kulichkov et al.*, 2008, 2010; *ReVelle*, 2010; *Chunchuzov et al.*, 2011] or due to discrepancies in the analysis related to large-scale phenomena, for example, the equinox [*Assink et al.*, 2014a] or a sudden stratospheric warming [*Smets and Evers*, 2014]. A current trend in improving infrasound propagation modeling is adding fine-scale structure and nonresolved gravity waves to one dimensional vertical profiles of horizontal wind, e.g., [*Drob et al.*, 2013]. As these modifications do not obey the physical laws acting in the atmosphere, for example, between wind and temperature, such adaptations are avoided in here.

However, the analysis excludes error variances of both model and observations. Therefore, we propose to model infrasound propagation based on an ensemble of realistically perturbed analyses provided by the European Centre for Medium-Range Weather Forecasts (ECMWF).

Infrasound, used as a verification technique for the Comprehensive Nuclear-Test-Ban Treaty (CTBT), has shown its ability to act as a passive technique to probe the upper atmosphere, e.g., [*Donn and Rind*, 1971; *Le Pichon et al.*, 2010; *Green et al.*, 2012; *Assink et al.*, 2012, 2014b, 2014a; *Smets and Evers*, 2014]. Both the treaty verification as well as atmospheric probing, e.g., inversion studies, make significant use of infrasound propagation

modeling that still relies on the deterministic estimate of the atmosphere. Usually, the analysis is used, but occasionally, modeling is based on free running atmospheric models that are not constrained by assimilating atmospheric observations. Therefore, this study contributes to improving the treaty verification and future atmospheric probing studies.

2. Realistic Atmospheric Perturbations

The analysis is a product of the data assimilation system, given as input an initial estimate field and a set of observations, defined by the time integration of the model equations from the previous analysis. However, the analysis provides a deterministic estimate of the true atmosphere, which can be off from the truth due to both model and observation errors.

At the European Centre for Medium-Range Weather Forecasts (ECMWF) the probability density function (PDF) of the atmosphere is sampled by an ensemble set of realistic perturbed analyses using the Ensemble Data Assimilation (EDA) system [*Buizza et al.*, 1999]. The ensembles are obtained by randomly perturbing the observations consistent with observational error statistics [*Houtekamer et al.*, 1996; *Houtekamer and Mitchell*, 2005], in combination with a stochastic backscatter scheme to simulate the effect of model uncertainties with amplitudes comparable to analysis error estimates [*Shutts*, 2005; *Berner et al.*, 2009]. For each observation apart from cloud-track winds, perturbations have been defined by randomly sampling a Gaussian distribution with zero mean and standard deviation defined by the observation error standard deviation [*Buizza et al.*, 2008]. Each perturbed analysis is produced using the same background error statistics in the four-dimensional variational data assimilation cycles [*Bonavita et al.*, 2012].

The ECMWF EDA ensemble of perturbed analyses with cycle 38r1 of the Integrated Forecasting System (IFS) consists of 25 ensemble members plus the unperturbed analysis, with a resolution of $T_L1279L137$ (horizontal resolution of ~16 km and 137 vertical levels up to 0.01 hPa). For infrasound propagation modeling, atmospheric specifications are used with a horizontal resolution of 0.1° which are vertically resampled to 500 m levels from ground up to 70 km. Ensembles of perturbed analyses are available every 12 h at noon and midnight UTC, respectively.

3. Infrasound Propagation Modeling

Sound is a pressure disturbance propagating through a medium, for example, air. Sound propagation through the medium is affected by the medium itself, which may result in either reflection or refraction and attenuation of the signal. The relation between density and pressure, affected by temperature (T), determines the adiabatic speed of sound (c) of the medium. Speed of sound is defined by the ideal gas law with adiabatic conditions, $c(\mathbf{x}) = \sqrt{\gamma RT(\mathbf{x})}$, with the ratio of specific heats for air $\gamma = c_p/c_v = 1.4$, the specific gas constant $R = 287$ J kg^{-1} K^{-1}, and position vector $\mathbf{x}$ inside the medium. The medium itself can be in motion, e.g., as wind in the atmosphere. Sound propagation is approximated by ray tracing, e.g., *Blom and Waxler* [2012]. In this study, a self-developed 3-D ray code for spherical coordinates is used. Ray equations for position $\mathbf{x}$ and slowness $\mathbf{s}$ are obtained from a canonical transformation of the high-frequency approximation of the wave equation using the Eikonal,

$$\dot{\mathbf{x}} = \mathbf{w}(1 - \mathbf{s}\cdot\mathbf{w}) - c^2\mathbf{s} \tag{1}$$

$$\dot{\mathbf{s}} = -c\frac{\mathrm{d}c}{\mathrm{d}\mathbf{x}}(\mathbf{s}\cdot\mathbf{s}) + (1 - \mathbf{s}\cdot\mathbf{w})\left(-\mathbf{s}\cdot\frac{\mathrm{d}\mathbf{w}}{\mathrm{d}\mathbf{x}}\right) \tag{2}$$

with 3-D wind vector $\mathbf{w}$. Along each ray the atmospheric attenuation (α) is obtained, including incoherent transmission loss due to geometrical spreading from the rays and frequency dependent absorption by the atmosphere, becoming more important with increasing altitude. Absorption, described by *Sutherland and Bass* [2004], depends on variations in thermal conductivity, density, viscosity, and relaxation throughout the medium and varying concentrations of chemical components. Incoherent transmission loss is described by the transport equation, based on the Jacobian determinant for ray coordinates azimuth and elevation [*Jensen et al.*, 2011].

Ray tracing is applied using full 3-D atmospheric specifications, interpolated by cubic splines with a smooth kernel. Eigenrays are obtained using a ray grid search method, evaluating all rays with elevation angles ranging from 0.0 to 45.0° with the horizontal in steps of 0.1° and azimuth angles ranging from 325.0 to 343.0° north

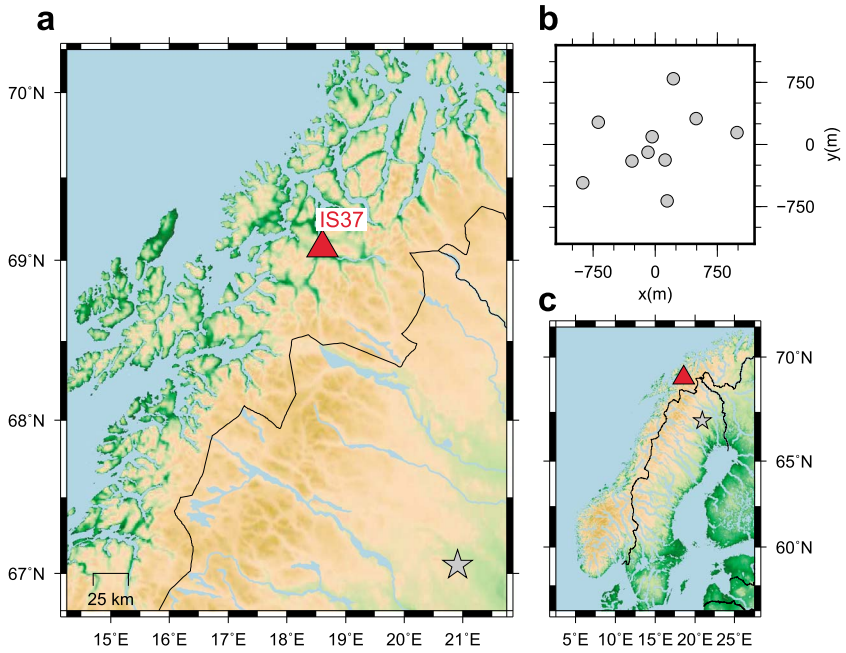

Figure 1. (a) Regional map indicating the location of IMS infrasound array IS37 (red triangle) in northern Norway and the location of the Aitik mine near Gällivare, northern Sweden: the site of large mining explosions. (b) Station layout of IS37. (c) Map of Norway and Sweden.

with steps of 0.1°. Eigenrays are defined as a ray approaching the array within 1.5 km Euclidean distance from the array center coordinate. Rays do not necessarily need to reflect at the surface but may refract close to the ground. Only stratospheric eigenrays are used, defined as eigenrays with a minimal ray refraction altitude of 20 km and a transmission loss below 100 dB re 1 km.

4. Case Study: One Year of Reference Events

Probabilistic infrasound propagation modeling is demonstrated by simulating 1 year of observed infrasound at array IS37 in Norway, part of the International Monitoring System (IMS) for verification of the Comprehensive Nuclear-Test-Ban Treaty (CTBT). Observed infrasound corresponds to mining activity in Aitik, e.g., blasting, near Gällivare, northern Sweden, at approximately 245 km distance. The location of the infrasound array IS37, its layout, and the location of the open pit mine are shown in Figure 1.

Locations and origin times are obtained from ground truth or GT events. A seismic signal with a known source is unambiguously associated with GT events using correlation detectors [*Gibbons and Ringdal*, 2006] and Empirical Matched Field Processing [*Harris and Kvaerna*, 2010], which are so-called pattern detectors. The uncertainty in the source location is limited to the dimensions of the mine (of the order of a couple of kilometers) [*Evers et al.*, 2012], and the origin time of each explosion can be determined to within approximately 1 s. All explosions take place at approximately 19:30 central European time (CET). Infrasound signals are detected by performing a channel-to-channel correlation procedure [cf. *Brown et al.*, 2002] using 10 s long segments of data in the 1–4 Hz band pass with 60% overlap. Figure 2 shows 358 associated observations of 46 events or mining explosions for 2014 in terms of travel time, trace velocity, and bearing deviation with respect to the back azimuth angle between IS37 and the ground truth source location. All associated events take place at approximately 19:30 CET.

To evaluate the added value of using realistic atmospheric perturbations, each of the associated events is simulated by 3-D ray tracing, see section 3. Conventional deterministic model predictions are obtained using the unperturbed analysis. Probabilistic infrasound predictions are described by a Monte Carlo method, aggregating the ray trace simulations of each individual ensemble member, sampling the PDF of the atmosphere. As the ensembles are only available every 12 h, eigenrays are simulated using the atmospheric specifications before and after the event to avoid temporal interpolation.

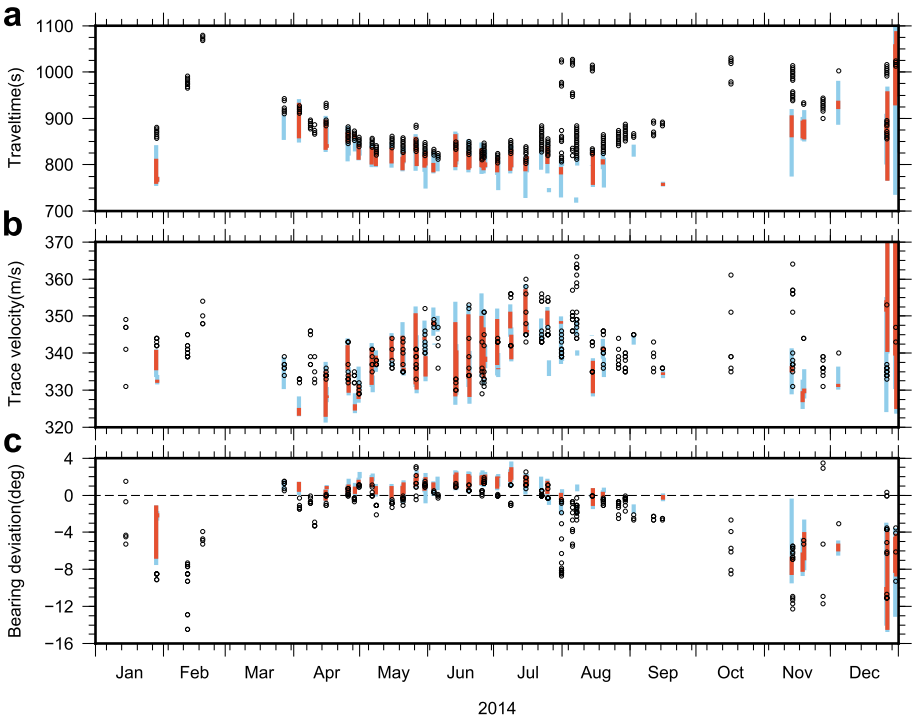

Figure 2. (a) Travel time, (b) trace velocity, and (c) bearing deviation of all infrasound events for IS37 corresponding with mining blasts at Aitikm near Gällivare in northern Sweden in 2014. Each panel shows (black circles) the observed signals, as well as the range of (vertical bar) the simulated signal characteristics obtained using (red) the analysis and (blue) the perturbations. Only stratospheric eigenrays within 1.5 km of the array central point are used.

5. Atmospheric Error Variance Profiles

Figure 3 shows 1 year of semidiurnal atmospheric ensemble spread profiles, an approximation of the error variance, for temperature (in terms of sound speed), wind direction and velocity, and effective sound speed in the direction from Gällivare. Vertical profiles correspond to the ensemble spread for the model grid point the nearest to the IS37 central coordinate. Figure 3 indicates an error increasing with height, in accordance with an increasing model and observational uncertainty as expected. However, at the stratopause, a sharp

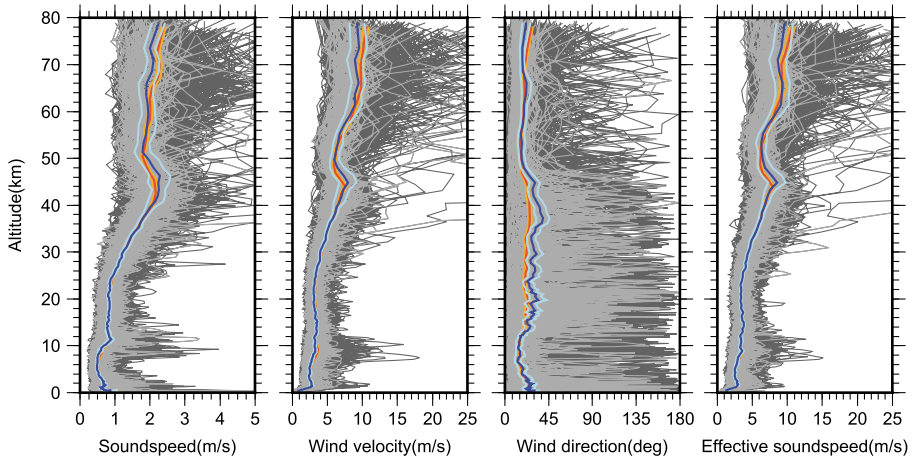

Figure 3. Ensemble spread at IS37 indicating error variance profiles for the year 2014 with 12 hour interval sampling. The profiles for the times at which signals from the Aitik events were observed are in light gray with profiles for all other times in dark grey. The mean error variance per level is shown in dark blue for the times of Aitik observations and red for all other times, and the 95% confidence intervals for times of observations and all other times are light blue and orange respectively.

Table 1. Number of Hits and Corresponding Hit Rates (Percentage) Between All 358 Observations and the Deterministic (Analysis) and Probabilistic (Ensemble) Ray Predictions[a]

	c_{app}		$\Delta\phi$		tt		all	
	Hits (Percentage)							
Analysis	93	(26.0%)	76	(21.2%)	84	(23.5%)	22	(6.1%)
Ensemble	183	(51.1%)	151	(42.2%)	127	(35.5%)	70	(19.6%)
Improvement	+90	(+96.8%)	+75	(+98.7%)	+43	(+51.2%)	+48	(+218.2%)

[a]Signal characteristics trace velocity (c_{app}), bearing deviation ($\Delta\phi$), and travel time (tt) are compared individually as well as combined (all).

decrease in variation is present, denoting the lack of assimilated observations. Below 25 km the variances for both wind and temperature are small and rather constant. Only the tropopause induces an increase in the temperature mean variance. Up to this altitude, still many data points using diverse observations techniques are assimilated [*Bouttier and Kelly*, 2001]. From 25 km and up to roughly 44 km, data assimilation is dominated by satellite based sounding, for example, nadir microwave sounding by Advanced Microwave Sounding Unit-A or limb sounding using GPS radio occultation. Distributions of temperature or other atmospheric properties, such as humidity or ozone content, are derived from radiative signals (see, for example, [*Rodgers*, 1976; *Healy and Thépaut*, 2006]). From 44 km up to 52 km the mean error variance is reduced significantly. This can be explained by the sudden decrease in the number of assimilated observations and the variety of the remote sensing techniques used. Consequentially, the atmospheric model is no longer constrained by observations but by climatology, resulting in a lower variance. Improving the analysis, and thus forecasts, involves resolving the stratosphere and assimilating upper atmospheric data [*Ramaswamy et al.*, 2001; *Gerber et al.*, 2009].

Effective sound speed variances are dominated by the error in wind strength and direction. The error variance for wind strength is approximately 4 times larger than the error variance for temperature. Ensemble spread profiles at the array indicate a yearly mean effective sound speed variation up to 8 ms^{-1} in the stratosphere, exceeding occasionally 25 ms^{-1} for a single ensemble set. In the mesosphere, the variation around the yearly mean sound speed error, of approximately 10 ms^{-1}, is significantly larger.

6. Deterministic Versus Probabilistic Simulations

Figure 2 shows the characteristics of the observed infrasound from the Aitik events, together with the ranges of signal characteristics predicted from the eigenrays using both the analysis and the ensemble of perturbed analyses. The performance of the model predictions is determined by the hit rate or probability of detection, defined by the number of observations correctly predicted divided by the total number of observations. An individual hit corresponds to an observed signal characteristic that falls within the range of the predicted signal characteristic. Similarly, a combined hit is evaluated, indicating an agreement of all three signal characteristics. False alarms are ignored. Hits and hit rates for the deterministic and the probabilistic simulations are listed in Table 1.

Model predictions using the analysis explain the general trend of the observations in summer. Between March and July most of the predictions agree with the observations. Some few predictions are obtained around the equinoxes, in winter, or in case of large back azimuth deviations. Prediction hit rates increase significantly when using EDA-based perturbations, as can be seen in Figure 2. In summer, almost all stratospheric observations coincide with the simulations, including the vernal equinox. Still, the overall performance is rather poor. Predicted travel times are predominantly lower than the observed travel times, and the observed bearing deviations are predominantly lower (more negative) than the predicted. The travel time prediction bias is most likely dominated by ray tracing issues. Late arrivals are probably a scattering or ray trace resolution issue, while the early predictions correspond with rays partly trapped in a tropospheric duct, which are not likely to be realistic. This results in a low probability of detection for travel time and, consequentially, a low hit rate for all combined characteristics. The Monte Carlo method using 26 ensembles generates a large number of predictions such that a probability distribution of the predicted signal characteristics can be determined.

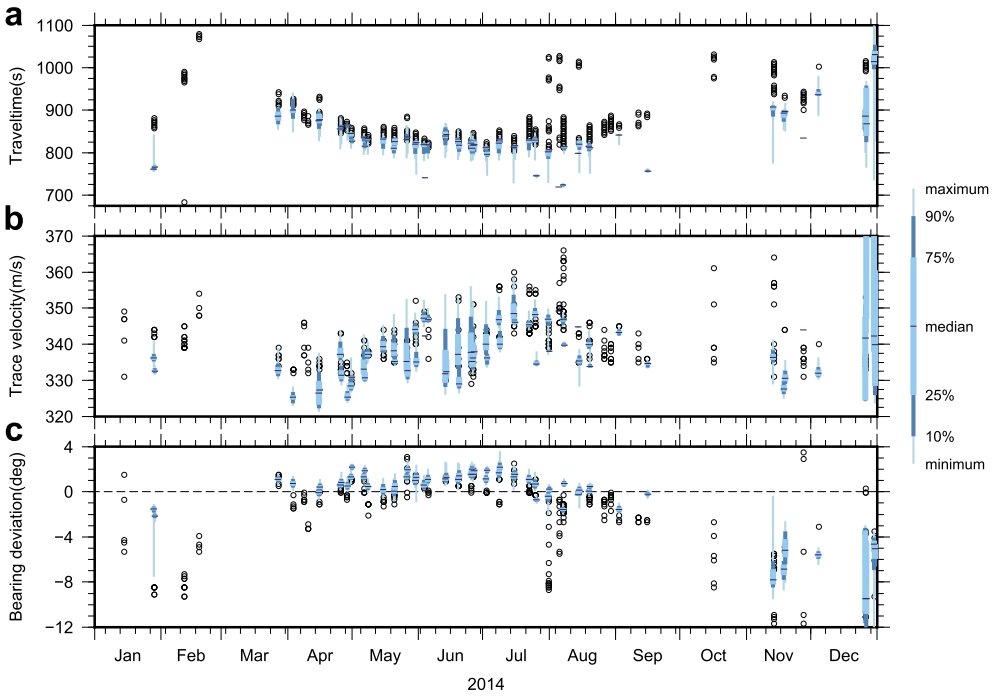

Figure 4. Percentile distribution of simulated events obtained using the atmospheric perturbations for signal characteristics (a) travel time, (b) trace velocity, and (c) bearing deviation. (black circles) Observed events at IS37 are shown in the background. For each simulated event the percentile distribution indicates the minimum, 10th centile, 25th centile, median, 75th centile, 90th centile, and the maximum.

This is shown in Figure 4 by the percentile distribution for each predicted signal characteristic. The obtained likelihood can be used to evaluate the performance of the simulated observations. Similarly, the percentile distribution is of importance to validate the atmospheric GCM, in this case including model and observational error variances.

An example is provided in the supporting information, Figure S1, which illustrates a day when the analysis fails to simulate the observed event while one of the ensemble members does succeed.

7. Discussion and Conclusions

In this study, the use of ensembles of realistically perturbed analyses for infrasound propagation modeling is successfully demonstrated. Although GCMs have limitations, a significant improvement in propagation modeling is obtained without the need of adding small-scale fluctuations. Error variance profiles at the array shown that the yearly mean effective sound speed variation can reach up to 8 ms^{-1} in the stratosphere, exceeding occasionally 25 ms^{-1} for a single ensemble set. The latter value is in the order of what other researchers have needed to explain infrasound observations, often dedicated to small-scale fluctuations and gravity waves [*Green et al.*, 2011; *Hedlin et al.*, 2012; *Drob et al.*, 2013] or model discrepancies [*Assink et al.*, 2014a].

Not all observations can be predicted, neither using the analysis nor by the ensemble of perturbed analyses, due to multiple reasons. First of all, neither upper mesospheric nor thermospheric observations can be simulated due to the altitude limit of the atmospheric model. Second, events originate around 19:30 CET, which is in the middle of two consecutive atmospheric realizations. As the analysis and perturbations before and after the event are used, with a time offset of 6 h, the atmosphere can be changed significantly during this time span. The time offset can be reduced using probabilistic forecasts provided by the Ensemble Prediction System (EPS) with 1 h steps. Third, a simulation can be missing due to limitations of the applied propagation modeling, ray tracing, which cannot penetrate the acoustic shadow zone as full wave models can, e.g., parabolic equation model [*Jensen et al.*, 2011]. Fourth, the ensemble of analyses can be off from the true state of the atmosphere. The bearing deviation prediction bias indicates that a bias in the analysis or ensemble can

be present. At last, differences can be related to the lack of physically plausible but unresolved small-scale fluctuations. Future research is required to determine whether or not the probabilistic approach will work as well for shorter source-to-station ranges, where simulations suggest that finite-frequency effects related to scattering from small-scale inhomogeneities generate much of the observed signal [*Kulichkov*, 2009].

Acknowledgments

This work was performed during the course of the ARISE design study (http://arise-project.eu), funded under the Seventh Framework Programme (FP7) of the European Union (grant 284387). The data for this paper from CTBTO and ECMWF are available to member states only but can be requested for academic purposes. Infrasound data can be requested at the CTBTO International Data Centre (IDC) in Vienna, via the virtual Data Exploration Centre (vDEC). Atmospheric data can be requested at the ECMWF via the Meteorological Archival and Retrieval System (MARS). The CTBTO and station operators are thanked for guaranteeing the high quality of the IMS data and products. Figures in this article were made with the Generic Mapping Tools [*Wessel and Smith*, 1991]. We thank D.N. Green and an anonymous reviewer for their reviews which helped in improving the manuscript.

The Editor thanks David Green and an anonymous reviewer for their assistance in evaluating this paper.

References

Assink, J. D., R. Waxler, and D. Drob (2012), On the sensitivity of infrasonic traveltimes in the equatorial region to the atmospheric tides, *J. Geophys. Res.*, *117*, D01110, doi:10.1029/2011JD016107.

Assink, J. D., A. L. Pichon, E. Blanc, M. Kallel, and L. Khemiri (2014a), Evaluation of wind and temperature profiles from ECMWF analysis on two hemispheres using volcanic infrasound, *J. Geophys. Res. Atmos.*, *119*, 8659–8683, doi:10.1002/2014JD021632.

Assink, J. D., R. Waxler, P. Smets, and L. G. Evers (2014b), Bidirectional infrasonic ducts associated with sudden stratospheric warming events, *J. Geophys. Res. Atmos.*, *119*, 1140–1153, doi:10.1002/2013JD021062.

Berner, J., G. J. Shutts, M. Leutbecher, and T. N. Palmer (2009), A spectral stochastic kinetic energy backscatter scheme and its impact on flow-dependent predictability in the ECMWF ensemble prediction system, *J. Atmos. Sci.*, *66*, 603–626.

Blom, P., and R. Waxler (2012), Impulse propagation in the nocturnal boundary layer: Analysis of the geometric component, *J. Acoust. Soc. Am.*, *131*, 3680–3690.

Bonavita, M., L. Isaksen, and E. Hólm (2012), On the use of EDA background error variances in the ECMWF 4D-Var, *Q. J. R. Meteorol. Soc.*, *138*, 1540–1559.

Bouttier, F., and G. Kelly (2001), Observing-system experiments in the ECMWF 4D-Var data assimilation system, *Q. J. R. Meteorol. Soc.*, *127*, 1469–1488.

Brown, D. J., C. N. Katz, R. Le Bras, M. P. Flanagan, J. Wang, and A. K. Gault (2002), Infrasonic signal detection and source location at the prototype international data centre, *Pure Appl. Geophys.*, *159*, 1081–1125.

Buizza, R., M. Milleer, and T. N. Palmer (1999), Stochastic representation of model uncertainties in the ECMWF ensemble prediction system, *Q. J. R. Meteorol. Soc.*, *125*, 2887–2908.

Buizza, R., M. Leutbecher, and L. Isaksen (2008), Potential use of an ensemble of analyses in the ECMWF Ensemble Prediction System, *Q. J. R. Meteorol. Soc.*, *134*, 2051–2066.

Chunchuzov, I., S. Kulichkov, A. Otrezov, and V. Perepelkin (2005), Acoustic pulse propagation through a fluctuating stably stratified atmospheric boundary layer, *J. Acoust. Soc. Am.*, *117*, 1868–1879.

Chunchuzov, I. P., S. N. Kulichkov, O. E. Popov, R. Waxler, and J. Assink (2011), Infrasound scattering from atmospheric anisotropic inhomogeneities, *Izv. Atmos. Ocean. Phys.*, *47*, 540–557.

Donn, W. L., and D. Rind (1971), Natural infrasound as an atmospheric probe, *Geophys. J. R. Astron. Soc.*, *26*, 111–133.

Drob, D. P., D. Broutman, M. A. Hedlin, N. W. Winslow, and R. G. Gibson (2013), A method for specifying atmospheric gravity wavefields for long-range infrasound propagation calculations, *J. Geophys. Res. Atmos.*, *118*, 3933–3943, doi:10.1029/2012JD018077.

Evers, L. G., A. R. J. van Geyt, P. Smets, and J. T. Fricke (2012), Anomalous infrasound propagation in a hot stratosphere and the existence of extremely small shadow zones, *J. Geophys. Res.*, *117*, D06120, doi:10.1029/2011JD017014.

Gerber, E. P., C. Orbe, and L. M. Polvani (2009), Stratospheric influence on the tropospheric circulation revealed by idealized ensemble forecasts, *Geophys. Res. Lett.*, *36*, L24801, doi:10.1029/2009GL040913.

Gibbons, S. J., and F. Ringdal (2006), The detection of low magnitude seismic events using array-based waveform correlation, *Geophys. J. Int.*, *165*, 149–166.

Green, D. N., J. Vergoz, R. Gibson, A. Le Pichon, and L. Ceranna (2011), Infrasound radiated by the Gerdec and Chelopechene explosions: Propagation along unexpected paths, *Geophys. J. Int.*, *185*, 890–910.

Green, D. N., R. S. Matoza, J. Vergoz, and A. L. Pichon (2012), Infrasonic propagation from the 2010 Eyjafjallajökull eruption: Investigating the influence of stratospheric solar tides, *J. Geophys. Res.*, *117*, D21202, doi:10.1029/2012JD017988.

Harris, D. B., and T. Kvaerna (2010), Superresolution with seismic arrays using empirical matched field processing, *Geophys. J. Int.*, *182*, 1455–1477.

Healy, S. B., and J. N. Thépaut (2006), Assimilation experiments with CHAMP GPS radio occultation measurements, *Q. J. R. Meteorol. Soc.*, *132*, 605–623.

Hedlin, M. A. H., C. de Groot-Hedlin, and D. Drob (2012), A study of infrasound propagation using dense seismic network recordings of surface explosions, *Bull. Seismol. Soc. Am.*, *102*, 1927–1937.

Houghton, J. T., L. Gylvan Meira Filho, D. J. Griggs, and K. Maskell (Eds.) (1997), An introduction to simple climate models used in the IPCC second assessment report, Tech. Rep., Intergovernemental Panel on Climate Change, Geneva, Switzerland.

Houtekamer, P. L., and H. L. Mitchell (2005), Ensemble Kalman filtering, *Q. J. R. Meteorol. Soc.*, *131*, 3269–3289.

Houtekamer, P. L., L. Lefaivre, J. Derome, H. Ritchie, and H. L. Mitchell (1996), A system simulation approach to ensemble prediction, *Mon. Weather Rev.*, *124*, 1255–1242.

Jensen, F. B., W. A. Kuperman, M. B. Porter, and H. Schmidt (2011), *Computational Ocean Acoustics (Modern Acoustics and Signal Processing)*, 2nd ed., Springer, New York.

Kulichkov, S. (2009), On the prospects for acoustic sounding of the fine structure of the middle atmosphere, in *Infrasound Monitoring for Atmospheric Studies*, edited by A. Le Pichon, E. Blanc, and A. Hauchecorne, chap. 16, pp. 511–540, Springer, New York.

Kulichkov, S. N., I. P. Chunchuzov, G. A. Bush, and V. G. Perepelkin (2008), Physical modeling of long-range infrasonic propagation in the atmosphere, *Izv. Atmos. Ocean. Phys.*, *44*, 175–186.

Kulichkov, S. N., I. P. Chunchuzov, and O. I. Popov (2010), Simulating the influence of an atmospheric fine inhomogeneous structure on long-range propagation of pulsed acoustic signals, *Izv. Atmos. Ocean. Phys.*, *46*, 69–77.

Le Pichon, A., E. Blanc, and A. Hauchecorne (Eds.) (2010), *Infrasound Monitoring for Atmospheric Studies*, 1st ed., pp. 629–646, Springer, New York.

Ramaswamy, V., et al. (2001), Stratospheric temperature trends: Observations and model simulations, *Rev. Geophys.*, *39*, 71–122.

Randall, D. A., et al. (2007), Climate models and their evaluation, in *Climate Change 2007: The Physical Science Basis. Contribution of Working Group I to the Fourth Assessment Report of the Intergovernmental Panel on Climate Change*, edited by S. Solomon et al., chap. 8, pp. 589–662, Cambridge Univ. Press, Cambridge, U. K., and New York.

ReVelle, D. O. (2010), Modified ray-mode (phase) theory: Understanding counter-wind propagation effects from atmospheric explosions, *J. Atmos. Sol. Terr. Phys.*, *72*, 241–261.

Rodgers, C. D. (1976), Retrieval of atmospheric temperature and composition from remote measurements of thermal radiation, *Rev. Geophys.*, *14*, 609–624.
Shutts, G. (2005), A kinetic energy backscatter algorithm for use in ensemble prediction systems, *Q. J. R. Meteorol. Soc.*, *131*, 3079–3102.
Shutts, G. J., and S. B. Vosper (2011), Stratospheric gravity waves revealed in NWP model forecasts, *Q. J. R. Meteorol. Soc.*, *137*, 303–317.
Smets, P. S. M., and L. G. Evers (2014), The life cycle of a sudden stratospheric warming from infrasonic ambient noise observations, *J. Geophys. Res. Atmos.*, *119*, 12,084–12,099, doi:10.1002/2014JD021905.
Sutherland, L. C., and H. E. Bass (2004), Atmospheric absorption in the atmosphere up to 160 km, *J. Acoust. Soc. Am.*, *115*, 1012–1032.
Wessel, P., and W. H. F. Smith (1991), Free software helps map and display data, *Eos. Trans. AGU*, *72*, 441–446.